ADVANCED OPTICAL MATERIALS
www.advopticalmat.de

Bio-Assisted Tailored Synthesis of Plasmonic Silver Nanorings and Site-Selective Deposition on Graphene Arrays

Giorgia Giovannini, Matteo Ardini, Nicolò Maccaferri, Xavier Zambrana-Puyalto, Gloria Panella, Francesco Angelucci, Rodolfo Ippoliti, Denis Garoli, and Francesco De Angelis**

The spontaneous interaction between noble metals and biological scaffolds enables simple and cost-effective synthesis of nanomaterials with unique features. Here, plasmonic silver nanorings are synthesized on a ring-like protein, i.e., a peroxiredoxin (PRX), and used to assemble large arrays of functional nanostructures. The PRX drives the seeding growth of metal silver under wet reducing conditions, yielding nanorings with outer and inner diameters down to 28 and 3 nm, respectively. The obtained hybrid nanostructures are selectively deposited onto a solid-state 2D membrane made of graphene in order to prepare plasmonic nanopores. In particular, the interaction between the graphene and the PRX allows for the simple preparation of ordered arrays of plasmonic nanorings on a 2D-material membrane. This fabrication process can be finalized by drilling a nanometer scale pore in the middle of the ring. Fluorescence spectroscopic measurements in combination with numerical simulations demonstrate the plasmonic effects induced in the metallic nanoring cavity. The prepared nanopores represent one of the first examples of hybrid plasmonic nanopore structures integrated on a 2D-material membrane. The diameter of the nanopore and the atomically thick substrate make this proof-of-concept approach particularly interesting for nanopore-based technologies and applications such as next-generation sequencing and single-molecule detection.

1. Introduction

Functional nanomaterials are drawing the attention of different scientific communities due to their unique mechanical,[1] magnetic,[2] electrical,[3] and optical[4] properties, which cannot be found in most of the corresponding bulk materials.[5–7] In this scenario, noble metallic nanostructures are intensively investigated for a wide range of applications such as electronics,[8] catalysis,[9] photonics,[10,11] sensing and biomedicine.[12–14] Among others, one of the most interesting phenomena related to metal-based nanostructures is their ability to couple with electromagnetic radiation and generate surface plasmons.[15,16] Surface plasmons can be used to engineer and localize electromagnetic fields, which find application in diverse fields, ranging from photonics to biosensing.[17]

Different approaches have been developed in order to prepare metallic nanostructures. Standard fabrication techniques, like thin-film deposition and nanolithography, exploit a "top-down" approach in which matter is sculpted and shaped until the desired final nanomaterial is achieved. Due to its robustness and efficiency, this method represents the main fabrication approach. Yet it is remarkably costly, both in terms of time and cost of the required facilities.[17,18] In contrast, bottom-up fabrication techniques offer the possibility to produce patterns on large scales at low costs.[19–21] One of these techniques is colloidal lithography.[22]

An alternative "bottom-up" approach that is quickly emerging as a valuable and cost-efficient strategy is based on the interaction between precursor molecules forming nanostructures.[23] In this context, nature provides several examples of self-assembling nanomaterials that can be applied to nanotechnology.[24,25] In particular, DNA and proteins are considered groundbreaking tools as they naturally self-assemble into several multi-level architectures.[26] Proteins are being explored for supramolecular chemistry applications and inspire the design of novel artificial nanomaterials fabricated by biotechnological, chemical, and computational expedients.[27,28] The access to ready-to-use protein assemblies with discrete structural patterns such as cages,[29] rings,[30] and tubes[31] is leading to promising results, for example, in magnetic resonance-based imaging.[32] As proteins, DNA has been used for similar purposes and

Dr. G. Giovannini, Dr. M. Ardini, Dr. N. Maccaferri, Dr. X. Zambrana-Puyalto, Dr. D. Garoli, Dr. F. De Angelis
Istituto Italiano di Tecnologia
via Morego 30, I-16163 Genova, Italy
E-mail: denis.garoli@iit.it; francesco.deangelis@iit.it
Dr. M. Ardini, Dr. G. Panella, Dr. F. Angelucci, Dr. R. Ippoliti
Department of Life
Health and Environmental Sciences
University of L'Aquila
Via Vetoio snc, Coppito, CAP 67100, L'Aquila, Italy
Dr. N. Maccaferri
Department of Physics and Material Sciences
Faculty of Science, Technology and Medicine
University of Luxembourg
162a, avenue de la Faïencerie, L-1511 Luxembourg, Luxembourg

The ORCID identification number(s) for the author(s) of this article can be found under https://doi.org/10.1002/adom.201901583.

DOI: 10.1002/adom.201901583

DNA origami finds now interesting applications as scaffold for nanofabrication.[33–39] Compared to DNA, proteins are more versatile thanks to their multiple anchoring sites, e.g., amino acids such as lysine, glutamate, and cysteine, ready for functionalization by means of amine, carboxyl, or thiol-reactive dyes, cross-linkers, and other biomolecules.[40,41] Note that in many proteins the carboxyl and amine-terminal residues lie along the surface of rim and cavity thus providing two very independent surfaces for biofunctionalization.[42] Moreover, protein data banks provide a large variety of shapes,[43] size,[26] surfaces,[44] and chemical properties, which can be used to achieve nanostructures with the desired morphology and features.[45]

In this context, ring-like proteins are likely to play a key role as they possess unique features, i.e., natural high abundance and remarkable structural stability.[46,47] In particular, 2-Cys peroxiredoxin (PRX) family members, such as the peroxiredoxin I from the human parasite *Schistosoma mansoni* (PRX), are particular intriguing. Ten identical subunits (≈25 kDa) of PRX, under reducing physiological conditions, associate into five dimers, which in turn undergo self-assembly into a large and stable ring-like complex (≈250 kDa) with thickness, and outer and inner diameters of 4.5, 12, and 6 nm, respectively (PDB code: 3ZTL).[44] Subunits interact in such a way that the PRX ring's bottom and top surfaces are identical thus providing a double-faced appearance, while the inner and outer surfaces of the ring present distinct features that can be exploited for different protein derivatization.[48]

Here we present a bio-assisted synthesis of plasmonic silver nanorings using the ring-like protein PRX as a scaffold (**Figure 1**). Electron microscopy, absorbance, and energy dispersion spectroscopy show that the surface amino acids of PRX can bind and arrange Ag^+ ions in aqueous solution to allow seeding growth of Ag^0 under wet reducing conditions to finally achieve the synthesis of nanorings with inner and outer diameters down to 28 and 3 nm, respectively (PRX-AgNRs). We demonstrate that these hybrid structures can be produced easily as colloidal suspension and integrated on-chip in order to prepare arrays of functional plasmonic nanostructures. In particular, we used the affinity between PRX and graphene to achieve a site selective deposition of PRX-AgNRs in large arrays (over hundreds of μm^2) of plasmonic cavities. The integration of metallic nanoparticles on graphene has been previously investigated.[38] Here, the controlled PRX deposition and synthesis of PRX-AgNRs in large arrays is demonstrated for the first time. The possibility to finalize the fabrication with a nanometer-scale pore in the graphene layer enables the fabrication of self-assembled plasmonic nanopores. This architecture enables significant electric field confinement within the nanopore cavity as demonstrated via numerical simulations and verified by fluorescence spectroscopy. We foresee that our proposed architecture might have a huge impact on nanopore-based technologies such as single-molecule detection and next-generation sequencing where nanopore sizes comparable to the typical size of the genomic and proteomic information are highly demanded.

2. Results and Discussion

2.1. Structural and Elemental Features of the PRX-AgNRs

PRX-AgNRs were synthesized exploiting a "bottom-up" approach based on wet chemistry. Ag^+ ions, formed by dissociation in water of the precursor $AgNO_3$, were first absorbed on the surface of PRX protein. Thanks to the ring-like conformation of the PRX protein, after reduction of the protein-bound metal by $NaBH_4$, PRX-AgNRs were achieved (see Figure 1).

The PRX-AgNRs have been examined by using transmission electron microscopy (TEM), as reported in **Figure 2**. Low magnification TEM micrographs showed the presence of electron-dense nanomaterials all over the carbon grid under different aggregation states likely due to the presence of metal (see also Note S1 in the Supporting Information). When increasing the magnification, single nanoparticles with non-spherical or elliptical architecture are observed, some of which clearly exhibit a hollow ring-like shape due to a visible inner cavity (Figure 2A). A collection of such ring-like nanoparticles allowed the estimation of the outer diameters of the cavity to be roughly between 32 and 25 nm and the inner ones between 6 and 1.9 nm with calculated average sizes of 28 ± 3 nm and 3.0 ± 1.3, respectively. It is worth mentioning here that several examples of metallic nanorings synthesis and fabrication have been reported in literature.[16,39,35,22,37] In almost all the cases[28] the size of the rings, in terms of outer and inner diameters, is in the scale of tens of nanometers, that is, an order of magnitude larger than the structures obtained here. Micrographs clearly show that the nanorings exhibit an apparent rough surface suggesting that metal seeding growth might have occurred during the synthesis. Energy dispersive spectroscopy (EDS) elemental analysis confirmed the presence of both PRX and silver within the nanorings. Indeed, the obtained color maps and related EDS spectra show the characteristic Ag signal (main peak at 3 keV) and other significant elements such as sulfur (S) and nitrogen (N), which

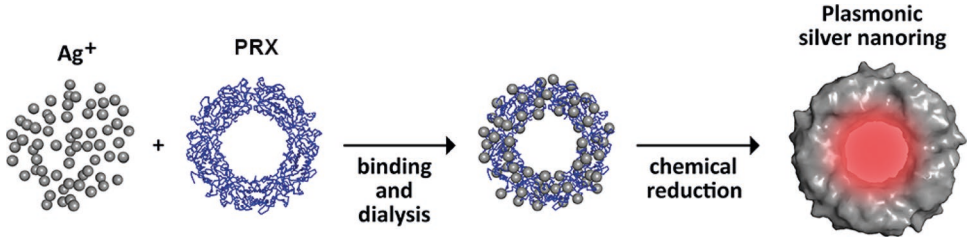

Figure 1. Outline of the PRX-AgNRs synthesis. The surface amino acids of the ring-like protein PRX (shown in blue ribbons) bind and spatially arrange Ag^+ ions. Chemical reduction of the protein-bound Ag^+ ions led to metal nanorings with an average diameter of 28 nm and a cavity of 3 nm.

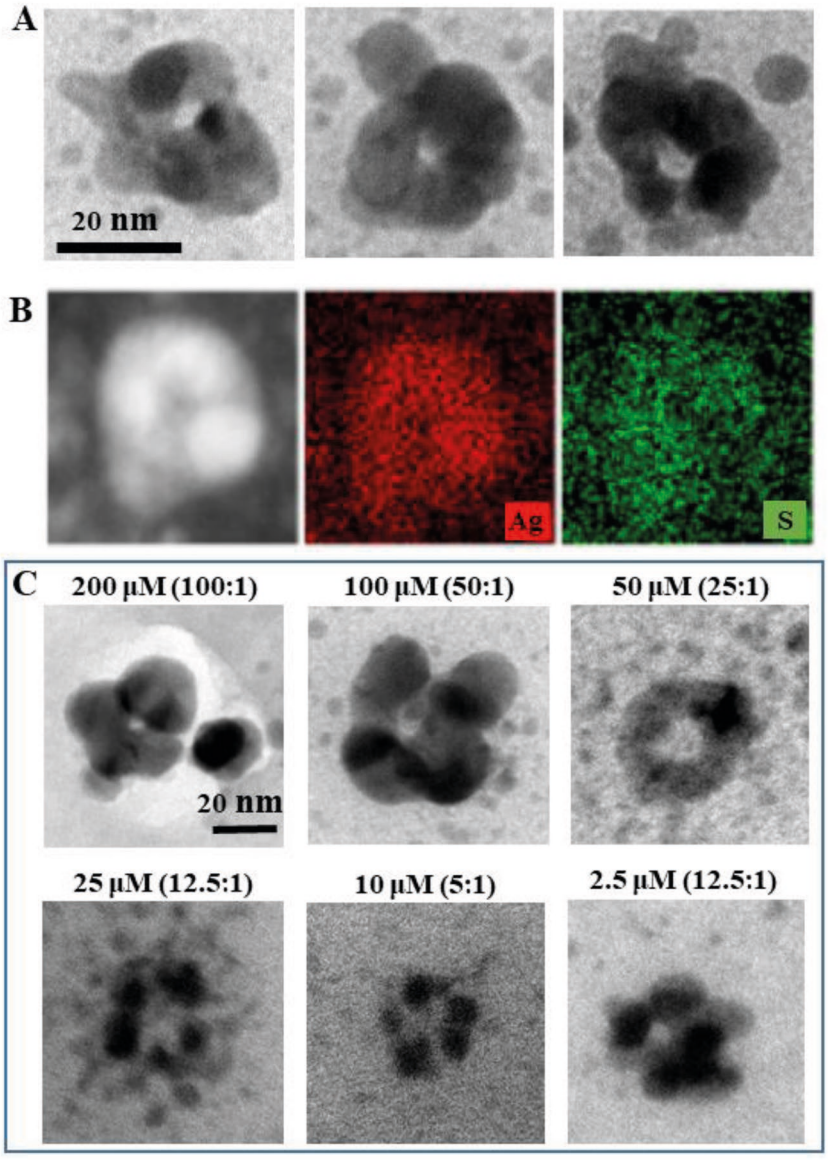

Figure 2. A) Ring-like nanoparticles having outer and inner diameter of 28 ± 3 nm and 3.0 ± 1.3 nm, respectively, synthesized using 100 as ratio $AgNO_3$:PRX. B) EDS analysis of Ag-PRX. Silver (red image) and sulfur (green image) are both detected for the ring-shaped nanomaterial indicating its hybrid metal-biocomposition. C) Example of PRX-AgNRs achieved by decreasing the amount of silver precursor used ($AgNO_3$).

were assigned to the protein's components, i.e., amino acids (see Figure 2B; and Note S1 and Figure S3, Supporting Information). These results clearly demonstrate the interaction between Ag and the PRX ring scaffold to achieve metal nanorings synthesis. Indeed, it is well known that the proteins' surface amino acids such as arginine, lysine, histidine, glutamate, methionine, and cysteine are effective anchoring sites for Ag+ ions,[1,49] which can be chemically reduced to Ag_0 precursors, perhaps small Ag_0 clusters, acting as seeds for other ions.[50]

The synthesis protocol was optimized in order to achieve a good yield of PRX-AgNRs and to limit the presence of undesired silver nanoparticles (AgNPs). First, considering the intrinsic reducing properties of citrate, different environmental conditions were tested for the synthesis. Dynamic light scattering analysis demonstrated that the reduction of Ag^+ and therefore the formation of AgNPs is limited using pure water instead of citrate buffer as dispersion solution (data not shown). However, the use of water during PRX-AgNRs synthesis led to not reproducible morphology as shown in Figure S4 (Supporting Information). These results demonstrate the importance of using citrate buffer (10×10^{-3} M, pH 5.5) for the production of nicely shaped PRX-AgNRs. Citrate buffer has presumably a double role in such situation: i) citrate ions stabilize the protein in its ring-like conformation during the synthesis and ii) Ag^+ is better absorbed on the protein surface likely due to the negative charge of citrate-coated protein. Due to the need of using citrate to stabilize the protein ring-like shape, the protocol was revisited varying the ratio of $AgNO_3$:PRX used. As shown in Figure 2C keeping constant the amount of protein used (2×10^{-6} M) and varying the amount of $AgNO_3$ (in the range between 2.5 and 200×10^{-6} M), PRX-AgNRs with the ring-like shape/morphology were achieved in almost all cases. On the contrary, keeping constant the amount of $AgNO_3$ (100×10^{-6} M) while changing the concentration of PRX led to metal PRX-AgNRs without a well-defined ring-like shape (see Note S1 and Figures S5 and S6 of the Supporting Information).

As expected, the lower the Ag^+:PRX ratio, the thinner was the silver layer over the protein surface. Most importantly, the use of low amount of Ag^+ allowed to improve the yield of the synthesis. As can be inferred by looking at the TEM micrographs of **Figure 3**, this optimization increased the amount of useful PRX-AgNRs while dramatically decreasing the amount of undesired AgNPs. The image shows that the number of PRX-AgNRs (red circles) is significantly higher compared to the undesired AgNPs (yellow circle), the latter showing very small diameters (≈2 nm). This is indeed a paramount result as the yield and the purity of the samples is crucial considering the final goal of this study that is their deposition on solid-state membrane and optimization of their plasmonic properties. From the analysis of the TEM images, we can state in a conservative way that using 2.5×10^{-6} M of $AgNO_3$ (ratio 1.25:1 Ag^+:PRX) ≈80% of the nanomaterial visible on the TEM grids can be identified as the wanted structures (PRX-AgNRs). This was a five-fold yield increase of the number of ring-shaped nanomaterials compared to that one obtained using 100×10^{-6} M $AgNO_3$ (ratio 50:1 Ag^+:PRX; ≈15%). Additional details are provided in Note S1, Figure S7A,B, and Table S1 of the Supporting Information.

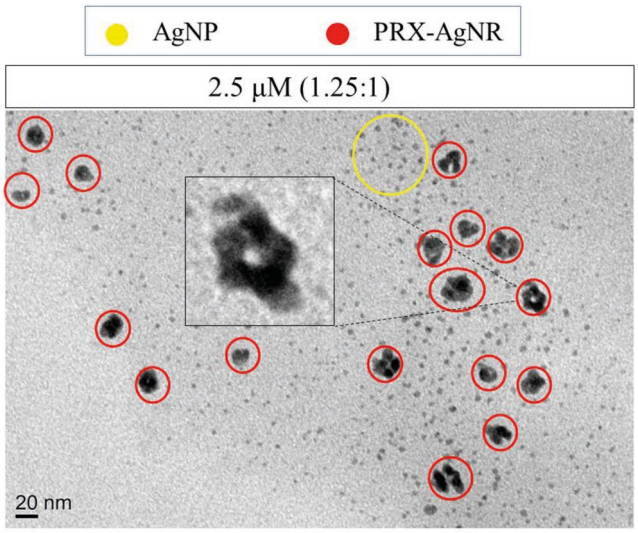

Figure 3. TEM image of sample prepared using 2.5×10^{-6} M of $AgNO_3$. Using low amount of $AgNO_3$, PRX-AgNRs (red circles) outnumber AgNPs (yellow circle), which are very small in size (≈2 nm).

2.2. Assembly of the PRX-AgNRs on Solid-State Membrane

Once the synthetic protocol in suspension was optimized, we focused the attention on the deposition of the PRX-AgNRs on a solid-state membrane. In principle, a simple drop casting can be used to prepare randomly distributed PRX-AgNRs as shown in Figure 3. Unfortunately, this is not suitable for nanotechnology applications that require well-organized nanostructures.[51]

In order to ensure an efficient site-selective deposition and to monitor every step of the process, i.e., deposition of PRX and successive AgNR formation/synthesis, we labeled the protein with a dye (Alexa647, suitable for fluorescent microscope analysis) and we optimized an in situ synthesis of PRX-AgNRs directly on the array. More in details, PRX was labeled using a PEGylated dye (PEG-Alexa647) and subsequently deposited on the membrane. The protocol used for protein labeling is described in the Experimental Section, whereas the UV–vis/fluorescence characterization of labeled-PRX can be found in Note S2, Figure S8, and Table S2 of the Supporting Information.

Two alternative approaches were evaluated for the site-selective deposition of labeled-PRX on the membrane: 1) chemical conjugation with di-thiol linker (see Note S3 of the Supporting Information) and 2) chemical affinity with 2D materials such as graphene. Best results were achieved using graphene as 2D material (reported in Figure 5). The design of the final structure is illustrated in **Figure 4**. It is worth noticing that the substrate was an array of metallic nanoholes with graphene flakes on the bottom (details of the substrate preparation are reported in the Experimental Section and in Note S5 of the Supporting Information). The presence of graphene in discrete sites enables the site-selective deposition of PRX-AgNRs. Graphene, in fact, is known to promote the stable deposition of PRX rings over the surface.[52] This is likely due to noncovalent biofunctionalization through van der Waals forces, electrostatics interactions, and/or π–π stacking.[53–55]

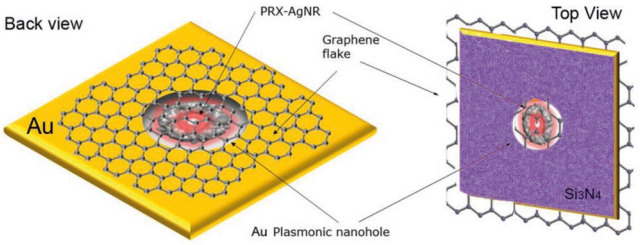

Figure 4. Cartoon of the prepared hybrid structure.

The possibility to synthesize PRX-AgNRs with the desired morphology starting from deposited PRX was first tested on simple carbon and graphene TEM grids (Note S5 and Figure S10, Supporting Information). Once the protocol was developed, the synthetic procedure was used for the preparation of the plasmonic nanostructures directly on labeled-PRX deposited on the graphene-decorated nanohole array. In particular, the labeled protein suspended in citrate buffer (2×10^{-6} M) was deposited onto graphene flakes exposed in the holes of the substrate by drop casting. After all solvent had evaporated, the unbound protein, if present, was removed by washing with water. $AgNO_3$ (5 μL, 2.5×10^{-6} M) was added on the substrate and after 30 min removed by washing and gently drying under nitrogen. $NaBH_4$ (5 μL, 2.5×10^{-6} M) was then added and after 10 min the substrate was finally washed with water.

By fluorescence confocal analysis it was then demonstrated that the in situ synthesis allows the localization of the nanostructure selectively in the holes of the arrays and that the fluorescence properties of the dye were not affected by the synthesis procedure (**Figure 5**). The properties of the fluorophore linked on the protein surface remained constant after silver coating as demonstrated by UV–vis analysis (Note S2 and Figure S8C, Supporting Information). As can be inferred from the TEM images (Figure 5C), PRX-AgNRs synthesized directly on the array were slightly larger in comparison to the one synthesized in suspension (Figure 3), with inner diameter of an average size value of 6.55 ± 2.75 nm. This can be explained by the favorable conditions present in correspondence of the nanoholes. Indeed, as it can be observed in the first image of Figure 5C (inset), AgNPs tend to form at the edge of the nanohole where artifacts of the substrate potentially induce the growth of metallic particles under mild conditions.[56] These small AgNPs can be included during the reduction of Ag^+ to Ag deposited on the protein surface thus resulting in the formation of PRX-AgNRs with larger diameter, filling all the space available in the hole.

It is worth mentioning here that the inner diameter of the plasmonic ring-like nanostructure, fundamental for the flow-through applications of the structure, remains intact. In particular, we verified that a 2 nm pore can be drilled in the center of the ring, through the graphene sheet on which the PRX-AgNRs lies, by means of TEM sculpturing[57] (see Note S5 and Figure S13 in the Supporting Information). Unfortunately, TEM-based procedures for nanopore fabrication are expensive and time consuming. On the contrary, alternative approaches driven by the plasmonic nanostructure[44,45] can be applied to our device. In fact, a plasmonic nanostructure on an atomic thin layer of graphene has been demonstrated to enable the self-aligned creating of pores.[58,59]

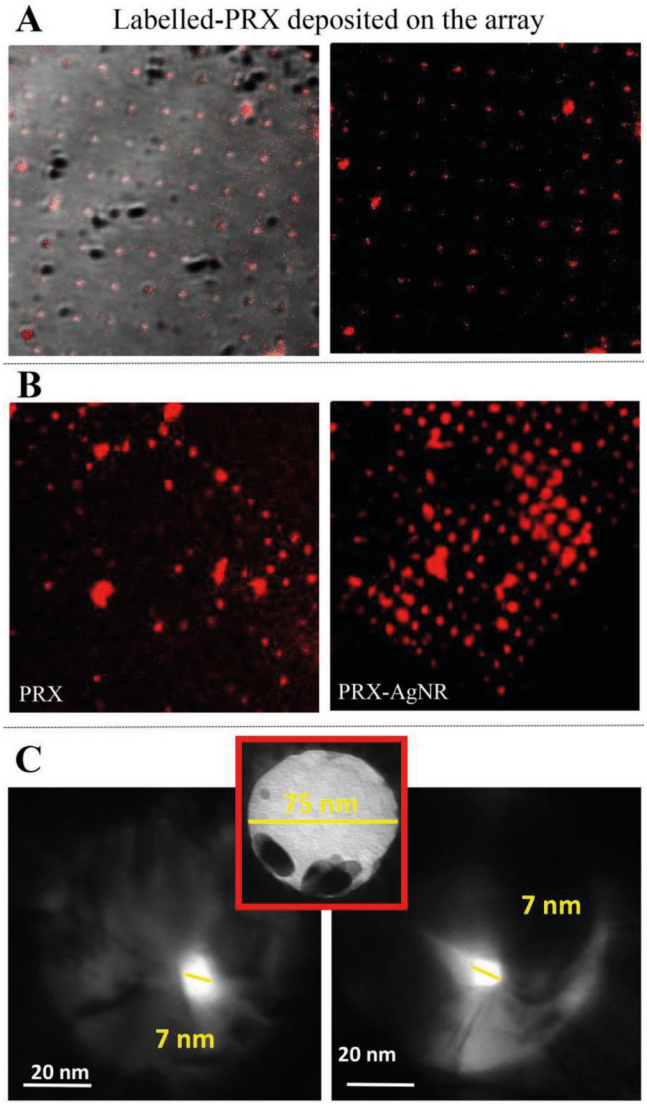

Figure 5. A) Confocal image of labeled-PRX with PEG-Alexa647 deposited on graphene-decorated nanohole array; The labeled-PRX is present in more than the 70% of the nanoholes. B) Confocal images of, respectively, labeled-PRX (left) and labeled-PRX-AgNRs (right). In both cases the fluorescence was localized on the hole of the array and the fluorescence is not altered by the in-situ synthesis of PRX-AgNRs. C) TEM images of PRX-AgNRs deposited on a single nanohole of the array. Image with red borders shows an explicative nanohole.

2.3. Plasmonic Effect of PRX-AgNRs: Fluorescent Enhancement

Labeling PRX with a fluorescent dye for site-selective deposition experiments allowed us to demonstrate the method of deposition as well as to probe the potential emission fluorescence enhancement (EE) given by the plasmonic field within the nanopore cavity. However, it is worth to note that two different dyes were used to acquire the images by confocal microscope (Alexa647) and for the EE measurements (ATTORho6G). The EE properties of the PRX-AgNR structures were evaluated carrying out a comparative lifetime analysis.[60] This method is independent from the number of emitting dyes and can be used to compare PRX and PRX-AgNRs directly. Using a home-made optical setup (see the Experimental Section), we computed the lifetime decay of the labeled PRX and the PRX-AgNR structures.

First of all, two samples with graphene-decorated nanohole arrays were fabricated. Separately, ATTORho6G labeled-PRX was deposited on the graphene-decorated nanohole arrays. In one of the two samples, labeled-PRX-AgNRs were successfully synthesized with the in situ protocol mentioned above. The lifetime of both samples was measured using our optical setup. Different nanoholes were measured for each sample. Noteworthy, the ring shape can play a crucial role in terms of lifetime spectra when elastic scattering is the dominant process.[61,62] In our case, due to the reduced dimensions of our rings compared to usual plasmonic nanostructures exceeding 100 nm, the absorption is the main process in this energy range, and the largest cross section in plasmon-assisted fluorescence emission corresponds to the process of optical absorption, so we are already in an optimal regime.[63] Tiny morphology changes/defects can affect the overall field enhancement due to the increased losses by a factor of two to three compared to the ideal perfectly ring-shaped structure, and the localization/confinement of the field. The obtained lifetimes were 2.3 ± 0.4 ns and 1.0 ± 0.8 ns for the PRX and the PRX-AgNRs, respectively. In **Figure 6**, two representative lifetime histograms are plotted. We found that the lifetime of the PRX-AgNRs was two times shorter than that of the PRX. This means that the emission of the ATTORho6G molecules is two times more efficient for the PRX-AgNRs structures. To note, the lifetime measurements are not enough to claim that there is a fluorescence enhancement, as the fluorescence is the combination of absorption and emission. Anyway, lifetime reduction, as well as local field enhancement, is a typical effect of plasmonic structures.[60] Thus, our measurements provide good evidence that plasmonic effects are present in the PRX-AgNR structures.

In order to better illustrate the expected plasmonic effects, we performed numerical simulations by using COMSOL Multiphysics considering: (i) an AgNR with dimension similar to the one measured in experiments (external and internal diameter of 28 and 3 nm, respectively) and (ii) the same AgNR deposited on a plasmonic cavity with graphene (Figure 4A). To note, as demonstrated by Wang and Shen[64] the shape is not crucial in determining the quality factor of a plasmon

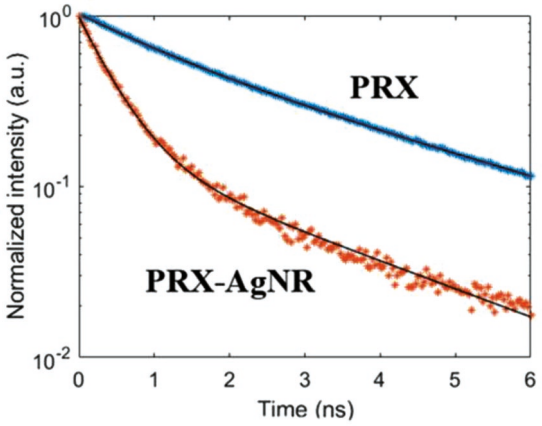

Figure 6. Lifetime spectra of dyes on PRX and PRX-AgNRs, respectively.

resonance, but its average dimension. Although the morphology of our AgNRs can slightly vary between different structures, it is always ring-like, so we decided to model our samples using a ring-shaped structure. The results are illustrated in Note S6 and Figures S14 and S15 of the Supporting Information. If a single AgNR is considered in H_2O, a significant electric field confinement with an intensity enhancement ($|E/E_0|^2$) of more than 300 can be achieved for an excitation wavelength of 532 nm. By changing the external diameter of the ring one can shift this plasmonic resonance to higher wavelengths, thus enabling a broadband control of the plasmonic enhancement in the nanopore. Finally, it is important to note that the AgNR suspended in H_2O is not suitable for a real application, but considering the same design deposited on a graphene layer inside a gold cavity the strong electric field confinement is preserved even if it is five times lower in intensity. Finally, with the nanopore placed on the graphene layer (as shown in Figure S12 of the Supporting Information), the simulation demonstrates that the field is highly confined, thus confirming the potential interest of this architecture for sequencing applications.

3. Conclusions

In this paper, we realized an optimized synthesis of silver nanorings (PRX-AgNRs) through an easy bio-assisted method where sub-5 nm nanopores can be prepared using PRX as template. The obtained ring-like nanostructures were selectively deposited on nanoholes arrays by exploiting the affinity of interaction between protein and graphene. As proof of concept, we tested the enhanced plasmonic properties of the designed metallic nanoring: a decrease of the fluorescent lifetime was observed confirming the expected plasmonic effect typically expected in these kinds of nanostructures. A 2 nm pore can be drilled in the inner hole of the PRX-AgNRs deposited on the 2D support. This can enable the flow-through of molecules in the plasmonic nanoring as, for instance, a linearized single strand DNA that is below 1 nm wide or a small globular protein molecule that is close to 2–1 nm.[65] The plasmonic properties of PRX-AgNRs integrated on the 2D membrane potentially allow the enhancement of signal measured from molecules flowing through the nanopore. The prepared structures represent one of the first examples of hybrid plasmonic nanopore integrated on a 2D-material membrane. The diameter of the nanopore and the atomically thick substrate make this proof-of-concept approach particularly interesting for nanopore-based technologies and applications such as next-generation sequencing and single-molecule detection.

4. Experimental Section

Bacterial Culture, SmPrxI (PRX) Expression, and Purification: PRX was obtained by heterologous expression as recombinant *N*-terminal 6-histidine protein according to literature.[38,66] Briefly, BL21(DE3) pLysS bacteria cells (Novagen) were transformed with a PRX-encoding plasmid and grown in selective LB medium (Sigma-Aldrich) before inducing the protein expression with IPTG (Sigma-Aldrich). Cells were harvested by centrifugation and suspended in tris(hydroxymethyl)aminomethane (TRIS) buffer pH 8.5 containing 150×10^{-3} M NaCl before lysis by sonication. A clarified cell extract was obtained by ultracentrifugation and loaded onto a nickel-bound affinity column connected to an ÄKTAprime plus chromatography system (GE Healthcare). The protein was stripped out by flushing with imidazole (Sigma-Aldrich) and its purity assessed through nonnative polyacrylamide gel electrophoresis (Sigma-Aldrich). The protein concentration was estimated by spectrophotometry according to a molar extinction coefficient and a ring molecular weight of 25440 M^{-1} cm^{-1} and 252.7 kDa, respectively. Ethylenediaminetetraacetic acid (EDTA) (EuroClone) and 2-ME (Sigma) were then added to remove any residual nickel and keep the protein in a ring conformation. Finally, the purified protein solution was sterilized by filter membranes (MDI Membrane Technologies, LLC) and stored at 4 °C up to 4 months. The protein concentration refers to the single subunit (25 kDa) throughout the text.

Silver Nanorings Synthesis: First, the purified PRX was dialyzed in 10×10^{-3} M sodium citrate buffer pH 5.5 (Sigma-Aldrich) for buffer exchange and removal of contaminants such as NaCl, EDTA, and β-ME. Citrate buffer at pH 5.5 was chosen since it guarantees a net electric charge of the protein to get stable in solution as the isoelectric point of PRX is 6.19 according to ExPASy ProtParam tool. Further, it is known that PRX undergoes various oligomeric transitions from low molecular dimeric species (≈50 kDa) to high molecular weight ring-shaped complexes (≈250 kDa) through chemical and physical stimuli. At acid pH of the citrate buffer (pH 5.5), the protein is stabilized as ring complex.[42] Dialysis was performed overnight at 8 °C using 15 kDa cutoff regenerated cellulose membranes (ThermoFisher Scientific) according to a volume ratio of 2500 (citrate buffer:PRX). The dialyzed protein was centrifuged 5 min at 10000 rpm at 8 °C to remove any aggregate and its concentration estimated by spectrophotometry (Nanodrop). The protein concentration was set at the desired concentration using citrate buffer as diluting solution. As a metal precursor, a stock solution of silver nitrate ($AgNO_3$, Sigma-Aldrich) in Milli-Q water was freshly made in a 1.5 mL low-adsorption tube (Sigma-Aldrich) and protected to light prior to use. Using 200 µL as final volume, 180 µL of PRX suspension was prepared at the desired protein concentration. To this solution 20 µL of $AgNO_3$ was added reaching the desired final concentration. In particular, $AgNO_3$ was added under shaking (500 rpm) at room temperature (RT; 20 °C) 5 µL over 10 min (5 µL x 4). **Table 1** shows the concentration of $AgNO_3$ and PRX, respectively, used in this study and the corresponding ratio. The protein concentration refers to the single subunit (25 kDa) throughout the text. Therefore, if the ring-protein is considered, the ratio $AgNO_3$:PRX will be always ten times higher than the one reported, which is related instead to the single protein unit since the concentration of ring-PRX is ten times lower than the one related to its single subunit.

Similarly, a buffered protein-free solution was made and used as control sample. Both samples were dialyzed 2 h at 8 °C under orbital shaking at 150 rpm in citrate buffer according to a volume ratio of 2500 (citrate buffer:sample) to remove the excess of Ag^+. After dialysis, a stock solution of reducing agent sodium borohydride ($NaBH_4$, Sigma-Aldrich) was freshly prepared in Milli-Q water in a low-adsorption tube and it was added to the dialyzed samples under constant shaking (500 rpm) to induce chemical reduction of silver. A total volume of 20 µL of $NaBH_4$ was added drop wise (5 µL × 4) over 10 min of constant shaking at RT

Table 1. Concentration of $AgNO_3$ and PRX, respectively, and the corresponding ratio.

Sample	$AgNO_3$ [$\times 10^{-6}$ M]	PRX [$\times 10^{-6}$ M]	$AgNO_3$:PRX
1	200	2	100
2	100	2	50
3	50	2	25
4	25	2	12.5
5	10	2	5
6	5	2	2.5
7	2.5	2	1.25
8	1	2	0.5

starting from a stock solution with specific concentration in order to achieve the desired concentration in the reaction. The final concentration of $NaBH_4$ always corresponded to the concentration of $AgNO_3$ previously chosen. Samples were then dialyzed against citrate buffer for 2 h. Note that citrate buffer was chosen as suitable diluting agent for $AgNO_3$ as other buffering reagents such as TRIS, 4-(2-hydroxyethyl)-1-piperazineethanesulfonic acid (HEPES), and 4-morpholinepropanesulfonic acid (MOPS) caused fast precipitation of the salt probably due to chelation of Ag+ ions and formation of insoluble complexes (data not shown).

Labeling of PRX: Depending upon the type of analysis, two different dyes were used to label the biological and hybrid materials: Alexa647, 651–672 nm as, respectively, $\lambda_{ex} - \lambda_{em}$ (Alexa Fluor 647 Succinimidyl Ester; ThermoFisher) was used for confocal imaging while ATTORho6G, 533–557 nm as, respectively, $\lambda_{ex} - \lambda_{em}$ (ATTO Rho6G Succinimidyl Ester; ATTO-TEC) was used for the evaluation of fluorescence lifetime.

In both cases, the dye was solubilized in 10×10^{-3} M phosphate-buffered saline pH 8 and NH_2-PEG-SH, 1 kDa (creative PEGWORKS) was added using as equivalent molar ration 1.5:1 (Dye:PEG). The reaction was shaken overnight at RT and finally dialysis was performed overnight at 8 °C using 300–500 Da cutoff regenerated cellulose membranes (ThermoFisher Scientific) to a volume ratio of 1000 (deionized water:PEGylatedDye).

10 µL of the PEGylated dye was added to the suspension of PRX (2×10^{-6} M) reaching 100×10^{-6} M as final concentration and the mixture was shaken (500 rpm) overnight at 8 °C. The biological/hybrid material was then purified by dialysis against 500 mL of citrate buffer using 15 kDa cutoff membrane for a minimum of 6 h. The so achieved labeled nanomaterials were characterized by spectrophotometric analysis (Tecan, Infinite M200).

In Situ Synthesis: Labeled-PRX was first deposited on the substrate (carbon/graphene TEM grids or membranes with graphene-decorated nanohole array): 5 µL of labeled-PRX at the desired concentration (2×10^{-6} M) was dropped on the substrate. Once the solvent evaporated, the substrate was washed by immersion in Milli-Q for 30 s and dried gently under nitrogen. Subsequently, 5 µL of $AgNO_3$ solution in citrate buffer at the desired concentration (2.5×10^{-6} M) was dropped on the substrate. After 30 min the grid was washed again, dried with nitrogen, and 5 µL of $NaBH_4$ (2.5×10^{-6} M) was dropped on the surface. After 5 min the substrate was finally washed and dried.

Bright-Field Transmission Electron Microscopy: Bright-field transmission electron microscopy (BF-TEM) imaging was carried out to investigate the morphology of samples by means of a JEM 1011 microscope (JOEL) equipped with a tungsten filament operating at 80 keV. To this aim, 2.5 µL (×2) of freshly prepared samples was dropped onto double carbon films (ultrathin carbon on holey carbon) on copper grids (Agar Scientific Ltd.) and let completely dry at room temperature under chemical hood. The grids were then rinsed three times with Milli-Q and gently dried with a mild nitrogen stream water before imaging by BF-TEM.

Preparation of Nanohole Array and Electrodeposition of Graphene Sheets: The substrate used for site-selective PRX deposition (illustrated in Figure 4) was prepared following procedure recently reported by our group.[67] In summary, an array of nanoholes was prepared by means of focused ion beam milling into a 100 nm thick Si_3N_4 membrane coated with 5//95 nm of Ti//Au. The diameter of the holes could be tuned by choosing the most suitable ion current; in our case holes of 60 nm were prepared. These nanoholes were then plugged with exfoliated graphene flakes[68] by using electrophoretic deposition.[67] An example of the prepared substrates is reported in Figure S11 of the Supporting Information. It is worth noting that the back side of the substrate was coated with gold (see Figure 4A), while the front side was coated with Si_3N_4. The graphene flakes were deposited on the gold layer, while the PRX was drop casted on the front side. This enabled the preferential deposition of PRX on graphene with respect to Si_3N_4 from where the PRX could be easily washed away.

Confocal Microscope Analysis: Labeled-PRX deposited on a graphene-decorated nanohole array and PRX-AgNRs synthesized in situ were imaged using a Nikon A1 confocal microscope. The structures were labeled with Alexa647 (651–672 nm $\lambda_{ex} - \lambda_{em}$). The images were taken with a laser at 640 nm, and the fluorescence was collected in the 650–700 nm range.

Fluorescence Lifetime Analysis: The fluorescence lifetime analysis of both the labeled-PRX deposited on a graphene-decorated nanohole array and the labeled PRX-AgNRs synthesized in situ was done using a noncommercial optical setup. An avalanche photodiode, as well as the picosecond laser at 532 nm, was connected to a time-correlated single-photon counting module in time-resolved mode. Making use of a home-built code, a histogram of 300 bins was built, each of them having a temporal width of 30 ps. A certain time delay was applied to the laser channel, so that the histogram was monotonously decreasing. The histogram measurement was carried out for 150 s. A biexponential function of the kind $Ae^{-t/\tau_A} + Be^{-t/\tau_B}$ was used to fit the decay curve. The lifetime was estimated as $\tau = \frac{(A\tau_A + B\tau_B)}{A+B}$. Each measurement was repeated several times, and the result was given as the average plus an uncertainty given by the standard deviation. More information on the optical setup can be looked up in our previous publication.[60] ATTORho6G dyes (533–557 nm $\lambda_{ex} - \lambda_{em}$) were used for the labeling.

Energy-Dispersive X-Ray Spectroscopy: Elemental analysis was carried out by energy-dispersive X-ray spectroscopy (EDS) by means of a Bruker XFlash5060 SDD system installed on the same TEM.

Numerical Simulations: Numerical simulations were carried out to investigate the optical response of the PRX-AgNRs. The electromagnetic response of an isolated nanoring was simulated using the finite-element method implemented in the RF Module of COMSOL Multiphysics. The dimensions of the outer and inner diameters of the rings were set according to the average sizes obtained from BF-TEM investigations (28 and 3 nm, respectively). The model computed the electric field of the nanoring. The unit cell was set to be 300 nm wide in *x*, *y* and *z*-directions, with perfect matching layers (200 nm thick) at the borders. An unpolarized plane wave impinged on the structure. In all the cases, the embedding medium was water (H_2O, $n = 1.33$).

UV–Visible Spectroscopy: UV–vis analysis of the formation of PRX-AgNRs in solution was analyzed recording the absorption scan (230–800 nm range) of the sample at each step of the synthesis. The synthesis was carried out in a quartz cuvette (Hellma) and the measurements were carried out with a Cary300 (Agilent).

Supporting Information

Supporting Information is available from the Wiley Online Library or from the author.

Acknowledgements

The research leading to these results received funding from the European Research Council under the Horizon 2020 Program, FET-Open: PROSEQO, Grant Agreement No. [687089]. We also acknowledge PON/FSE R&I (No. AIM1887574) from MIUR-Ministero dell'Istruzione, dell'Università e della Ricerca (Ministry of Education, University and Research) to support M.A.

Conflict of Interest

The authors declare no conflict of interest.

Author Contributions

G.G. and M.A. contributed equally to this work. G.G. and M.A. fabricated and characterized the structures; N.M. performed the numerical simulations; X.Z.-P. performed the optical microscope analysis; G.P., F.A., and R.I. synthetized and optimized the PRX; and D.G. and F.D.A. supervised the work.

Keywords

hybrid-nanomaterials, nanopores, plasmonics, selective-deposition, silver nanorings

Received: September 19, 2019
Revised: November 3, 2019
Published online:

[1] Y. Wang, Y. Mei, F. Huang, X. Yang, Y. Li, J. Li, F. Meng, Z. Zhou, *Carbon* **2019**, *147*, 490.
[2] K. Mandal, D. Jana, B. K. Ghorai, N. R. Jana, *ACS Appl. Nano Mater.* **2019**, *2*, 3292.
[3] S. Sagadevan, M. Priya, *J. Nano Res.* **2015**, *30*, 1.
[4] M.-M. Yin, W.-Q. Chen, Y. Liu, F.-L. Jiang, *ACS Appl. Nano Mater.* **2019**, *2*, 408.
[5] A. G. N. Sofiah, M. Samykano, K. Kadirgama, R. V. Mohan, N. A. C. Lah, *Appl. Mater. Today* **2018**, *11*, 320.
[6] S. Kim, J.-M. Kim, J.-E. Park, J.-M. Nam, *Adv. Mater.* **2018**, *30*, 1704528.
[7] J. Lee, O. Adegoke, E. Y. Park, *Biotechnol. J.* **2019**, *14*, 1800249.
[8] Z. Yin, B. Wang, G. Chen, M. Zhan, *J. Mater. Sci.* **2011**, *46*, 2397.
[9] X. Qian, C. Xu, Y. Jiang, J. Zhang, G. Guan, Y. Huang, *Chem. Eng. J.* **2019**, *368*, 202.
[10] T. K. Pathak, H. C. Swart, R. E. Kroon, *Phys. B* **2018**, *535*, 114.
[11] Y. Chen, Z. Fan, Z. Zhang, W. Niu, C. Li, N. Yang, B. Chen, H. Zhang, *Chem. Rev.* **2018**, *118*, 6409.
[12] M. G. Manera, A. Colombelli, A. Taurino, A. G. Martin, R. Rella, *Sci. Rep.* **2018**, *8*, 12640.
[13] D. Cassano, S. Pocoví-Martínez, V. Voliani, *Bioconjugate Chem.* **2018**, *29*, 4.
[14] D. Garoli, H. Yamazaki, N. Maccaferri, M. Wanunu, *Nano Lett.* **2019**, *19*, 7553.
[15] S. A. Maier, *Plasmonics: Fundamentals and Applications*, Springer, New York, NY **2007**.
[16] R. Near, C. Tabor, J. Duan, R. Pachter, M. El-Sayed, *Nano Lett.* **2012**, *12*, 2158.
[17] M. I. Stockman, K. Kneipp, S. I. Bozhevolnyi, S. Saha, A. Dutta, J. Ndukaife, N. Kinsey, H. Reddy, U. Guler, V. M. Shalaev, A. Boltasseva, B. Gholipour, H. N. S. Krishnamoorthy, K. F. MacDonald, C. Soci, N. I. Zheludev, V. Savinov, R. Singh, P. Groß, C. Lienau, M. Vadai, M. L. Solomon, D. R. Barton, M. Lawrence, J. A. Dionne, S. V. Boriskina, R. Esteban, J. Aizpurua, X. Zhang, S. Yang, D. Wang, W. Wang, T. W. Odom, N. Accanto, P. M. De Roque, I. M. Hancu, L. Piatkowski, N. F. Van Hulst, M. F. Kling, *J. Opt.* **2018**, *20*, 043001.
[18] M. J. Kelly, *Nanotechnology* **2011**, *22*, 245303.
[19] J. B. Reeves, R. K. Jayne, L. Barrett, A. E. White, D. J. Bishop, *Nanoscale* **2019**, *11*, 3261.
[20] M. Cesaria, A. Taurino, M. G. Manera, M. Minunni, S. Scarano, R. Rella, *Nanoscale* **2019**, *11*, 8416.
[21] H. Fredriksson, Y. Alaverdyan, A. Dmitriev, C. Langhammer, D. S. Sutherland, M. Zäch, B. Kasemo, *Adv. Mater.* **2007**, *19*, 4297.
[22] J. Ye, P. Van Dorpe, L. Lagae, G. Maes, G. Borghs, *Nanotechnology* **2009**, *20*, 465203.
[23] N. Giuseppone, *Acc. Chem. Res.* **2012**, *45*, 2178.
[24] B. A. Grzybowski, W. T. S. Huck, *Nat. Nanotechnol.* **2016**, *11*, 585.
[25] I. Ocsoy, D. Tasdemir, S. Mazicioglu, C. Celik, A. Katı, F. Ulgen, *Mater. Lett.* **2018**, *212*, 45.
[26] B. J. G. E. Pieters, M. B. van Eldijk, R. J. M. Nolte, J. Mecinović, *Chem. Soc. Rev.* **2016**, *45*, 24.
[27] S. E. Ahnert, J. A. Marsh, H. Hernández, C. V Robinson, S. A. Teichmann, *Science* **2015**, *350*, aaa2245.
[28] S. S. Bayram, O. K. Zahr, J. Del Re, A. S. Blum, *Nanotechnology* **2016**, *27*, 485603.
[29] M. Ardini, B. D. Howes, A. Fiorillo, E. Falvo, S. Sottini, D. Rovai, M. Lantieri, A. Ilari, D. Gatteschi, G. Spina, E. Chiancone, S. Stefanini, M. Fittipaldi, *J. Inorg. Biochem.* **2018**, *182*, 103.
[30] F. Saccoccia, P. Di Micco, G. Boumis, M. Brunori, I. Koutris, A. E. Miele, V. Morea, P. Sriratana, D. L. Williams, A. Bellelli, F. Angelucci, *Structure* **2012**, *20*, 429.
[31] C. R. Noël, F. Cai, C. A. Kerfeld, *Adv. Mater. Interfaces* **2016**, *3*, 1500295.
[32] M. A. Kostiainen, P. Ceci, M. Fornara, P. Hiekkataipale, O. Kasyutich, R. J. M. Nolte, J. J. L. M. Cornelissen, R. D. Desautels, J. van Lierop, *ACS Nano* **2011**, *5*, 6394.
[33] F. A. S. Engelhardt, F. Praetorius, C. H. Wachauf, G. Brüggenthies, F. Kohler, B. Kick, K. L. Kadletz, P. N. Pham, K. L. Behler, T. Gerling, H. Dietz, *ACS Nano* **2019**, *13*, 5015.
[34] A. A. Zinchenko, K. Yoshikawa, D. Baigl, *Adv. Mater.* **2005**, *17*, https://doi.org/10.1002/adma.200590121.
[35] E.-M. Roller, L. Khosravi Khorashad, M. Fedoruk, R. Schreiber, A. O. Govorov, T. Liedl, *Nano Lett.* **2015**, *15*, 1368.
[36] C. T. Wirges, J. Timper, M. Fischler, A. S. Sologubenko, J. Mayer, U. Simon, T. Carell, *Angew. Chem., Int. Ed.* **2009**, *48*, 219.
[37] I. Ocsoy, M. L. Paret, M. Arslan Ocsoy, S. Kunwar, T. Chen, M. You, W. Tan, *ACS Nano* **2013**, *7*, 8972.
[38] I. Ocsoy, B. Gulbakan, T. Chen, G. Zhu, Z. Chen, M. M. Sari, L. Peng, X. Xiong, X. Fang, W. Tan, *Adv. Mater.* **2013**, *25*, 2319.
[39] A. A. Zinchenko, K. Yoshikawa, D. Baigl, *Adv. Mater.* **2005**, *17*, 2820.
[40] V. Chabert, M. Hologne, O. Sénèque, A. Crochet, O. Walker, K. M. Fromm, *Chem. Commun.* **2017**, *53*, 6105.
[41] K. M. Fromm, *CHIMIA Int. J. Chem.* **2014**, *67*, 851.
[42] F. Angelucci, F. Saccoccia, M. Ardini, G. Boumis, M. Brunori, L. Di Leandro, R. Ippoliti, A. E. Miele, G. Natoli, S. Scotti, A. Bellelli, *J. Mol. Biol.* **2013**, *425*, 4556.
[43] R. A. McMillan, J. Howard, N. J. Zaluzec, H. K. Kagawa, R. Mogul, Y.-F. Li, C. D. Paavola, J. D. Trent, *J. Am. Chem. Soc.* **2005**, *127*, 2800.
[44] F. Angelucci, A. E. Miele, M. Ardini, G. Boumis, F. Saccoccia, A. Bellelli, *Mol. Biochem. Parasitol.* **2016**, *206*, 2.
[45] S. Manuguri, K. Webster, N. A. Yewdall, Y. An, H. Venugopal, V. Bhugra, A. Turner, L. J. Domigan, J. A. Gerrard, D. E. Williams, J. Malmström, *Nano Lett.* **2018**, *18*, 5138.
[46] F. Ippoliti, R. Ardini, M. Di Leandro, L. Giansanti, F. Cimini, A. Ottaviano, L. Morandi, V. Ortolani, L. Angelucci, in *GraphITA*, **2017**, 1.
[47] A. Schreiber, M. C. Huber, H. Cölfen, S. M. Schiller, *Nat. Commun.* **2015**, *6*, 6705.
[48] F. Angelucci, A. Bellelli, M. Ardini, R. Ippoliti, F. Saccoccia, V. Morea, *FEBS J.* **2015**, *282*, 2827.
[49] T. Shoeib, K. W. Michael Siu, A. C. Hopkinson, *J. Phys. Chem. A* **2002**, *106*, 6121.
[50] J. Polte, X. Tuaev, M. Wuithschick, A. Fischer, A. F. Thuenemann, K. Rademann, R. Kraehnert, F. Emmerling, *ACS Nano* **2012**, *6*, 5791.
[51] Y. Wu, K. Zhang, B. Yang, *Adv. Opt. Mater.* **2019**, *7*, 1800980.
[52] M. Ardini, G. Golia, P. Passaretti, A. Cimini, G. Pitari, F. Giansanti, L. Di Leandro, L. Ottaviano, F. Perrozzi, S. Santucci, V. Morandi, L. Ortolani, M. Christian, E. Treossi, V. Palermo, F. Angelucci, R. Ippoliti, *Nanoscale* **2016**, *8*, 6739.
[53] Y. Kamiya, K. Yamazaki, T. Ogino, *J. Colloid Interface Sci.* **2014**, *431*, 77.
[54] Z. Gu, Z. Yang, L. Wang, H. Zhou, C. A. Jimenez-Cruz, R. Zhou, *Sci. Rep.* **2015**, *5*, 10873.
[55] Y. Taniguchi, T. Miki, Y. Ohno, M. Nagase, Y. Arakawa, Y. Imada, K. Minagawa, M. Yasuzawa, *Jpn. J. Appl. Phys.* **2019**, *58*, 055001.
[56] D. Garoli, D. Mosconi, E. Miele, N. Maccaferri, M. Ardini, G. Giovannini, M. Dipalo, S. Agnoli, F. De Angelis, *Nanoscale* **2018**, *10*, 17105.

[57] F. Börrnert, L. Fu, S. Gorantla, M. Knupfer, B. Büchner, M. H. Rümmeli, *ACS Nano* **2012**, *6*, 10327.
[58] S. Pud, D. Verschueren, N. Vukovic, C. Plesa, M. P. Jonsson, C. Dekker, *Nano Lett.* **2015**, *15*, 7112.
[59] S. Nam, I. Choi, C. Fu, K. Kim, S. Hong, Y. Choi, A. Zettl, L. P. Lee, *Nano Lett.* **2014**, *14*, 5584.
[60] X. Zambrana-Puyalto, N. Maccaferri, P. Ponzellini, G. Giovannini, F. De Angelis, D. Garoli, *Nanoscale Adv.* **2019**, *1*, 2454.
[61] F. Tam, G. P. Goodrich, B. R. Johnson, N. J. Halas, *Nano Lett.* **2007**, *7*, 496.
[62] R. F. Aroca, G. Yi Teo, H. Mohan, A. R. Guerrero, P. Albella, F. Moreno, *J. Phys. Chem. C* **2011**, *115*, 20419.
[63] J.-F. Li, C.-Y. Li, R. F. Aroca, *Chem. Soc. Rev.* **2017**, *46*, 3962.
[64] F. Wang, Y. R. Shen, *Phys. Rev. Lett.* **2006**, *97*, 206806.
[65] K. Briggs, H. Kwok, V. Cossa, *Small* **2014**, *10*, 2077.
[66] A. A. Sayed, D. L. Williams, *J. Biol. Chem.* **2004**, *279*, 26159.
[67] D. Mosconi, G. Giovannini, A. Jacassi, P. Ponzellini, N. Maccaferri, P. Vavassori, M. Serri, M. Dipalo, D. Darvill, F. De Angelis, S. Agnoli, D. Garoli, *ACS Omega* **2019**, *4*, 9294.
[68] A. E. Del Rio Castillo, V. Pellegrini, A. Ansaldo, F. Ricciardella, H. Sun, L. Marasco, J. Buha, Z. Dang, L. Gagliani, E. Lago, N. Curreli, S. Gentiluomo, F. Palazon, M. Prato, R. Oropesa-Nuñez, P. S. Toth, E. Mantero, M. Crugliano, A. Gamucci, A. Tomadin, M. Polini, F. Bonaccorso, *Mater. Horiz.* **2018**, *5*, 890.